Takagi-Sugeno Multimodeling-Based Large Signal Stability Analysis of DC Microgrid Clusters

Sucheng Liu, *Member, IEEE*, Xiang Li, *Student Member, IEEE*, Mengyu Xia, *Student Member, IEEE*, Qiangdong Qin, *Student Member, IEEE*, and Xiaodong Liu

***Abstract*—DC microgrid (DCMG) clusters represent interconnections of multiple DCMGs to enable flexible power flow, and hence advantages of high resilience, economic dispatch, loss minimization, and optimal load response with microgrid-based distributed generations can fully be taken. However, small-scale DCMGs are known to be weak in nature due to low inertia and high grid impedance. Meanwhile, dynamic analyses of DCMG clusters have been plagued by their high order dynamic nonlinear system models since numerous state variables are involved. This article proposes large signal stability analysis of DCMG clusters based on Takagi-Sugeno multimodeling approach. With the proposed method, the large signal Lyapunov stability of the DCMG cluster is reduced to the computation of a series of linear matrix inequalities, which will significantly simplify the analysis. The influences of circuit parameters, power flows, and topological change on large signal stability of the DCMG cluster are revealed, and asymptotic stability regions of the network are estimated as well. In addition to simulation verification, a laboratory prototype of a ring topology DCMG cluster with three 48 V DCMGs interconnected is also built to validate the analysis by experimental results.**

***Index Terms*—DC microgrid (DCMG) clusters, large signal stability, nonlinear system, Takagi-Sugeno (T-S) fuzzy model.**

Nomenclature

r_{it}	Resistance of *i*th tie-line.
L_{it}	Inductance of *i*th tie-line.
i_{it}	Current flows through *i*th tie-line.
V_i	Equivalent dc source representing *i*th DCMG.
r_i	Equivalent resistance of the line in *i*th DCMG.
L_i	Equivalent inductance of the line in *i*th DCMG.
i_i	Current flows through inductor (L_i).
C_i	Capacitance of the dc bus for the *i*th DCMG.
$v_{\mathrm{bus}i}$	Bus voltage of *i*th DCMG.
R_i	Resistance of the CIL in *i*th DCMG.
$I_{\mathrm{CCL}i}$	Current of the CCL in *i*th DCMG.
$P_{\mathrm{CPL}i}$	Power of the CPL in *i*th DCMG.
$i_{\mathrm{o}i}$	Current of the generic load in *i*th DCMG.

Manuscript received December 31, 2020; revised March 25, 2021; accepted April 20, 2021. Date of publication April 30, 2021; date of current version July 30, 2021. This work was supported in part by the Natural Science Foundation of China under Grant 51407003 and in part by Anhui Higher Education Institutions of China under Project KJ2019A0066. Recommended for publication by Associate Editor M. Hartmann. (*Corresponding author: Sucheng Liu.*)

The authors are with the Key Laboratory of Power Electronics and Motion Control, Anhui University of Technology, Ma'anshan 243032, China (e-mail: liusucheng@gmail.com; lixiang96@ahut.edu.cn; ayu224215@163.com; qinqiangdong@ahut.edu.cn; liuxiaodong@ahut.edu.cn).

Color versions of one or more figures in this article are available at https://doi.org/10.1109/TPEL.2021.3076734.

Digital Object Identifier 10.1109/TPEL.2021.3076734

I. Introduction

In THE last decades, the progress of dc power conversion technologies has promoted the resurgence of dc-based power applications, especially in the distributed generation field. In this background, dc microgrids (DCMGs) have emerged as attractive solutions for renewable energy applications to achieve a number of benefits, such as high efficiency, low cost, and simple control design, and so forth [1]–[3]. Furthermore, neighboring dc microgrids can be interconnected as complementary to each other to form DCMG clusters, also referred to as networked DCMGs that enabling flexible power flows, and hence advantages of high resilience, economic dispatch, loss minimization, and optimal load response with microgrid-based distributed generations can fully be taken [4]–[8].

However, DCMGs those consisting of renewable energy sources (RESs), e.g., photovoltaic (PV) array and wind turbine, energy storage systems, e.g., battery and supercapacitor, and electronic load, are often in small scales at tens or hundreds of kilowatts, which are known as weak grids due to low inertia and high grid impedance. Therefore, DCMGs are easy to be disturbed by various transient events, such as intermittence of the RESs, load switching, short-circuit fault, and so forth [9]–[11]. In this sense, DCMG clusters can be considered as "weak-weak" interconnections of DCMGs, which will cause more serious stability problems than a single DCMG due to decreased damping. On the other hand, dynamic analyses of DCMG clusters have been plagued by their high order dynamic nonlinear system models since numerous state variables and multiple nonlinear components, e.g., constant power loads (CPLs) or switching behavior, are involved.

Presently, there are only a few works on the analysis of DCMG clusters in small signal cases. Moreover, modeling and analysis of DCMG clusters in large signal conception can hardly be found. In [12], the local Lyapunov functions are derived based on the multi-input multi-output linear state-space model of the DCMG cluster, where the asymptotic stability of the system with the proposed primary plug-and-play and secondary leader-based controllers is guaranteed. In [13], the small signal model of the DCMG cluster is developed with simplified transfer functions of each dc microgrid so that the influence of CPL and inductance of the tie-line on the small signal stability of the system can be

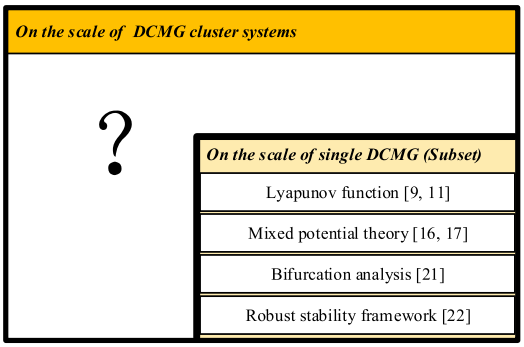

Fig. 1. Overview of large signal stability studies on DCMG clusters.

observed by the root locus. A similar method as using transfer functions to evaluate and design small signal stability of the ac microgrid clusters is found in [14]. Nevertheless, small signal analysis can only predict system dynamic behavior in a small region around the equilibrium point. Unfortunately, the existing works still lack large signal stability analysis of DCMG clusters, and it turns out that much focus is primarily on single DCMG instead of the complete interconnected cluster systems.

Fig. 1 briefly shows an overview of large signal stability studies on DCMG cluster systems, where the single DCMG can be considered as a subset of complete DCMG cluster systems, and fruitful methods have been deployed to analyze large signal stability at the scale of the single DCMG. The pioneering analysis on large signal stability of a distributed power system with CPL was carried out in [15] where the mixed potential function was developed as the stability criteria in the Lyapunov stability context. Since then, the CPL-induced large signal stability problems have been extensively dealt with in the cascaded power systems, and recently in dc microgrids [16]. In [17], the conservatism of the mixed potential theory in large signal stability criterion of the dc microgrid is improved with the refined models for the CPL converter, but only the extracted cascaded converter model is considered as the case of study, and hence the other aspects of the operation of the dc microgrid are absent. In [10], [18], and [19], the droop control is included in the large signal stability analysis of the dc microgrid. The large signal stability of the dc microgrid is also investigated at the common coupling of point with particular attention was paid to estimation of the grid impedance [20]. The bifurcation diagram is deployed to assist the stability analysis of equilibrium points of the dc microgrid under droop control [21]. The sufficient criteria for large-signal stability in dc microgrids with distributed-controlled dc-dc power converters are rigorously derived with mathematically proved confidence, and the defects with the mixed potential function are resolved as well [9]. The robust stability framework is proposed for the dc microgrid by considering the uncertainty of the CPL [22]. The Takagi-Sugeno (T-S) fuzzy system modeling approach is introduced to analyze the large signal stability of the voltage source inverter for driver application [23]. All these works promote the advances of large signal stability of single DCMG. But modeling and analysis on the scale of DCMG cluster systems with multiple microgrids interconnected rather than single DCMG, especially in large signal notion, are still lacking.

Herein, the lack of large signal stability analysis on DCMG clusters motivates the work, and the major contributions of the article are mentioned as follows.

1) The T-S multimodeling approach, new in its application in DCMG clusters, is first time introduced to perform large signal stability analysis of the higher-order nonlinear dynamic network. The quadratic Lyapunov functions that facilitate large signal stability analysis of the DCMG cluster are easily computed with the help of the T-S multimodeling approach, and the regions of asymptotic stability (RASs) are also estimated with considered scenarios.
2) A comprehensive analysis of the DCMG cluster is conducted. The power flows of the DCMG cluster in the steady-state operation are highlighted to point out the unique characteristics of the system with respect to the single DCMG. Furthermore, not only the influences of circuit parameters on the large signal stability analysis are revealed, but the power flow and the topological variation from ring to star interconnection are included as well.
3) In addition to simulation results, a laboratory prototype of a ring topology DCMG cluster with three 48 V dc microgrids is built to experimentally corroborate the analysis results.

The rest of the article is organized as follows. Section II performs modeling of the DCMG cluster. Section III proposes the large signal stability analysis approach based on T-S fuzzy modeling for the DCMG cluster system. Section IV presents the large signal stability analysis of the DCMG cluster with the specific topology and the given parameters. Section V verifies the analysis by both simulations and experimental results. Finally, Section VI concludes the article.

II. Modeling of the DC Microgrid Cluster

The DCMG cluster with the general interconnection of multiple DCMGs is shown in Fig. 2 where each DCMG consists of the PV system and the battery energy storage system, and the generic load as shown in Fig. 2(a), and the topology with the interconnection of n DCMGs, i.e., DCMG1, DCMG2, …, and DCMGn, by tie-lines are depicted in Fig. 2(b), respectively. Due to negligible parasitic capacitances, the tie-line can be represented by a series connection of line resistance and inductance without loss of generality [24].

A. Equivalent Model of the Single DCMG

In practical applications, the load of the dc microgrid is usually a CPL, that is, represented from the input of a tightly controlled dc/dc or dc/ac converters. Seeing from the dc bus side, the CPL presents nonlinear and negative impedance characteristics, which has a significant destabilizing effect [25], [26]. Therefore, CPL has been considered as the primary source of instability in the study of large signal stability of dc power systems [9]–[11], [15], [16]. However, ZIP load that consists of constant impedance load (CIL, Z), constant current load (CCL, I), and CPL (P) connected in parallel is considered as a generic

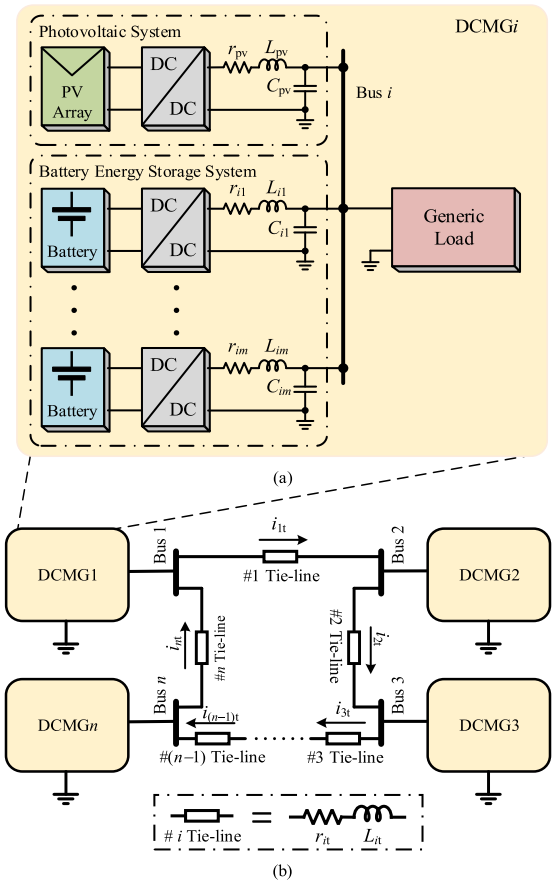

Fig. 2. Configuration of the DCMG cluster. (a) Single DCMG. (b) General DCMG cluster topology.

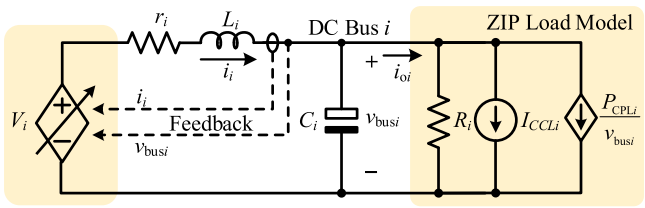

Fig. 3. Equivalent model of the single DCMG with generic ZIP load.

nonlinear load connected to the bus of each DCMG for a more general case [12].

On the other hand, the DCMG cluster system is composed of multiple interconnected DCMGs, hence they are complex dynamic systems with high order and multiple nonlinear elements, which poses a grand challenge for the large signal stability analysis for the system. Fortunately, the power flow of the DCMG cluster is usually dictated by the tertiary level in the hierarchical control paradigm [27], which is of low-frequency dynamics so that reduced-order modeling of the DCMG cluster is possible by ignoring high-frequency dynamics [10], [20], [28].

Fig. 3 illustrates the equivalent model of each DCMG where the controlled voltage source V_i stands for the regulated dc bus voltage in no-load condition, and r_i, L_i, and C_i denote the line resistance, the line inductance, and the capacitance of the dc bus of the reduced-order model of the single DCMG, respectively, and i_{oi} represents the current of the ZIP load. The current flows through and the voltage across the load can be expressed as

$$\begin{cases} i_{oi} = \underbrace{\dfrac{v_{busi}}{R_i}}_{\text{CIL}} + \underbrace{I_{CCLi}}_{\text{CCL}} + \underbrace{\dfrac{P_{CPLi}}{v_{busi}}}_{\text{CPL}} \\ v_{busi} = \dfrac{R_i(i_{oi}-I_{CCLi}) - \sqrt{(R_i(i_{oi}-I_{CCLi}))^2 - 4R_i P_{CPLi}}}{2}. \end{cases} \tag{1}$$

B. Complete Modeling of the DCMG Cluster

Given the equivalent model of the single DCMG, the complete model of the DCMG cluster can be derived in a straightforward way by piecing together the equivalent circuit models of the interconnected DCMGs by the tie-lines. Then, the dynamics of the $(3 \times n)$th-order system model for the DCMG cluster can be described as

$$\begin{cases} \left.\begin{aligned} &L_1\tfrac{di_1}{dt} = -r_1 i_1 - v_{bus1} + V_1 \\ &L_2\tfrac{di_2}{dt} = -r_2 i_2 - v_{bus2} + V_2 \\ &\vdots \\ &L_n\tfrac{di_n}{dt} = -r_n i_n - v_{busn} + V_n \end{aligned}\right\} \text{Inductor current of each DCMG} \\ \left.\begin{aligned} &L_{1t}\tfrac{di_{1t}}{dt} = -r_{1t} i_{1t} + v_{bus1} - v_{bus2} \\ &L_{2t}\tfrac{di_{2t}}{dt} = -r_{2t} i_{2t} + v_{bus2} - v_{bus3} \\ &\vdots \\ &L_{nt}\tfrac{di_{nt}}{dt} = -r_{nt} i_{nt} + v_{busn} - v_{bus1} \end{aligned}\right\} \text{Inductor currents of the tie - lines} \\ \left.\begin{aligned} &C_1\tfrac{dv_{bus1}}{dt} = i_1 + i_{nt} - i_{1t} \\ &-\tfrac{P_{CPL1}}{v_{bus1}} - \tfrac{v_{bus1}}{R_1} - I_{CCL1} \\ &C_2\tfrac{dv_{bus2}}{dt} = i_2 + i_{1t} - i_{2t} \\ &-\tfrac{P_{CPL2}}{v_{bus2}} - \tfrac{v_{bus2}}{R_2} - I_{CCL2} \\ &\vdots \\ &C_n\tfrac{dv_{busn}}{dt} = i_n + i_{(n-1)t} - i_{nt} \\ &-\tfrac{P_{CPLn}}{v_{busn}} - \tfrac{v_{busn}}{R_n} - I_{CCLn} \end{aligned}\right\} \text{Bus voltage of each DCMG.} \end{cases} \tag{2}$$

The power difference can be expressed as follows when the CPL*i* has step transient

$$\Delta P_{CPLi} = P^*_{CPLi} - P_{CPLi} \tag{3}$$

where P_{CPLi} and P^*_{CPLi} denote the power of the CPL*i* before step transient, and the power of the CPL*i* after step transient, respectively.

The dc bus voltages will also move to new equilibrium points when the CPLs have step transient, so the dc bus voltages can be estimated as follows in this transition

$$v_{busi} = V_{busi} - \left(\underbrace{\frac{v_{busi} - V_{busi}}{R_i}}_{\text{CIL}} + \underbrace{\frac{\Delta P_{CPLi}}{v_{busi}}}_{\text{CPL}} \right) r_i \tag{4}$$

where V_{busi} and v_{busi} represent the dc bus voltage before the CPL*i* step transient and the dc bus voltage after the CPL*i* step transient, respectively.

Solving (4) will depend on two conditions as follows.

1) R_i is connected in parallel to the dc bus, the bus voltage is solved as

$$v_{\mathrm{bus}i}=\frac{V_{\mathrm{bus}i}+\sqrt{{V_{\mathrm{bus}i}}^2-4\frac{r_iR_i}{r_i+R_i}\Delta P_{\mathrm{CPL}i}}}{2} \tag{5}$$

where $\Delta P_{\mathrm{CPL}i}<\frac{(r_i+R_i){V_{\mathrm{bus}i}}^2}{4r_iR_i}$.

1) R_i is open-circuited, the solution becomes

$$v_{\mathrm{bus}i}=\frac{V_{\mathrm{bus}i}+\sqrt{{V_{\mathrm{bus}i}}^2-4r_i\Delta P_{\mathrm{CPL}i}}}{2} \tag{6}$$

where $\Delta P_{\mathrm{CPL}i}<\frac{{V_{\mathrm{bus}i}}^2}{4r_i}$.

If the CPLs have step transient, then the changed values of the dc bus voltage will be introduced into the system model for stability analysis. For simplicity, the equilibrium points of (2) are shifted to the origin (zero) of the state space, and new state variables are defined as

$$\begin{cases} x_1=i_1-I_1^0\\ x_2=i_2-I_2^0\\ \vdots\\ x_n=i_n-I_n^0\\ x_{n+1}=i_{1\mathrm{t}}-I_{1\mathrm{t}}^0\\ x_{n+2}=i_{2\mathrm{t}}-I_{2\mathrm{t}}^0\\ \vdots\\ x_{2n}=i_{n\mathrm{t}}-I_{n\mathrm{t}}^0\\ x_{2n+1}=v_{\mathrm{bus}1}-V_{\mathrm{bus}1}^0\\ x_{2n+2}=v_{\mathrm{bus}2}-V_{\mathrm{bus}2}^0\\ \vdots\\ x_{3n}=v_{\mathrm{bus}n}-V_{\mathrm{bus}n}^0 \end{cases} \tag{7}$$

where I_i^0 , $I_{i\mathrm{t}}^0$, and $V_{\mathrm{bus}i}^0$ are the steady-state values (operating points) of the variables.

The corresponding state-space model of the DCMG cluster is given by

$$\dot{\mathbf{x}}=f(\mathbf{x},\mathbf{u})=\left[\begin{array}{c|c|c} A_{k-1} & O_{n\times n} & A_{k-2}\\ \hline O_{n\times n} & A_{k-3} & A_{k-4}\\ \hline A_{k-5} & A_{k-6} & A_{k-7} \end{array}\right]\cdot\mathbf{x}+\left[\begin{array}{c|c|c} B_{k-1} & O_{n\times n} & O_{n\times n}\\ \hline O_{n\times n} & O_{n\times n} & O_{n\times n}\\ \hline O_{n\times n} & O_{n\times n} & B_{k-2} \end{array}\right]\cdot\mathbf{u} \tag{8}$$

where f is a nonlinear function due to the CPL in (2), and the state vector and the input vector are represented by $\mathbf{x}=[\,x_1\ \cdots\ x_n\ x_{n+1}\ \cdots\ x_{2n}\ x_{2n+1}\ \cdots\ x_{3n}\,]^T$, and $\mathbf{u}=[\,V_1\ \ldots\ V_n\ \underbrace{0\cdots 0}_{n}\ -I_{\mathrm{CCL}1}\ \cdots\ -I_{\mathrm{CCL}n}\,]^T$, respectively.

The sub-matrices in (8) are expressed as follows:

$$A_{k-1}=\begin{bmatrix} -\frac{r_1}{L_1} & 0 & \cdots & 0\\ 0 & -\frac{r_2}{L_2} & \ddots & \vdots\\ \vdots & \ddots & \ddots & 0\\ 0 & \cdots & 0 & -\frac{r_n}{L_n} \end{bmatrix} \tag{9-a}$$

$$A_{k-2}=\begin{bmatrix} -\frac{1}{L_1} & 0 & \cdots & 0\\ 0 & -\frac{1}{L_2} & \ddots & \vdots\\ \vdots & \ddots & \ddots & 0\\ 0 & \cdots & 0 & -\frac{1}{L_n} \end{bmatrix} \tag{9-b}$$

$$A_{k-3}=\begin{bmatrix} -\frac{r_{1\mathrm{t}}}{L_{1\mathrm{t}}} & 0 & \cdots & 0\\ 0 & -\frac{r_{2\mathrm{t}}}{L_{2\mathrm{t}}} & \ddots & \vdots\\ \vdots & \ddots & \ddots & 0\\ 0 & \cdots & 0 & -\frac{r_{n\mathrm{t}}}{L_{n\mathrm{t}}} \end{bmatrix} \tag{9-c}$$

$$A_{k-4}=\begin{bmatrix} \frac{1}{L_{1\mathrm{t}}} & -\frac{1}{L_{1\mathrm{t}}} & 0 & \cdots & 0\\ 0 & \frac{1}{L_{2\mathrm{t}}} & -\frac{1}{L_{2\mathrm{t}}} & \ddots & \vdots\\ \vdots & \ddots & \ddots & \ddots & 0\\ 0 & \ddots & 0 & \frac{1}{L_{(n-1)\mathrm{t}}} & -\frac{1}{L_{(n-1)\mathrm{t}}}\\ -\frac{1}{L_{n\mathrm{t}}} & 0 & \cdots & 0 & \frac{1}{L_{n\mathrm{t}}} \end{bmatrix} \tag{9-d}$$

$$A_{k-5}=\begin{bmatrix} \frac{1}{C_1} & 0 & \cdots & 0\\ 0 & \frac{1}{C_2} & \ddots & \vdots\\ \vdots & \ddots & \ddots & 0\\ 0 & \cdots & 0 & \frac{1}{C_n} \end{bmatrix} \tag{9-e}$$

$$A_{k-6}=\begin{bmatrix} -\frac{1}{C_1} & 0 & \cdots & 0 & \frac{1}{C_1}\\ \frac{1}{C_2} & -\frac{1}{C_2} & 0 & \ddots & 0\\ \vdots & \ddots & \ddots & \ddots & \vdots\\ 0 & \ddots & \frac{1}{C_{(n-1)}} & -\frac{1}{C_{(n-1)}} & 0\\ 0 & 0 & \cdots & \frac{1}{C_n} & -\frac{1}{C_n} \end{bmatrix} \tag{9-f}$$

$$A_{k-7}=\begin{bmatrix} G(x_{2n+1}) & 0 & \cdots & 0\\ 0 & G(x_{2n+2}) & \ddots & \vdots\\ \vdots & \ddots & \ddots & 0\\ 0 & \cdots & 0 & G(x_{3n}) \end{bmatrix} \tag{9-g}$$

$$B_{k-1}=\begin{bmatrix} \frac{1}{L_1} & 0 & \cdots & 0\\ 0 & \frac{1}{L_2} & \ddots & \vdots\\ \vdots & \ddots & \ddots & 0\\ 0 & \cdots & 0 & \frac{1}{L_n} \end{bmatrix} \tag{9-h}$$

$$B_{k-2}=\begin{bmatrix} \frac{1}{C_1} & 0 & \cdots & 0\\ 0 & \frac{1}{C_2} & \ddots & \vdots\\ \vdots & \ddots & \ddots & 0\\ 0 & \cdots & 0 & \frac{1}{C_n} \end{bmatrix}. \tag{9-i}$$

Moreover, the nonlinear functions in (9-g) are described as

$$\begin{cases} G(x_{2n+1})=\frac{P_{\mathrm{CPL}1}^0}{C_1V_{\mathrm{bus}1}^0}\cdot g(x_{2n+1})-\frac{1}{C_1R_1}\\ \vdots\\ G(x_{3n})=\frac{P_{\mathrm{CPL}n}^0}{C_nV_{\mathrm{bus}n}^0}\cdot g(x_{3n})-\frac{1}{C_nR_n}. \end{cases} \tag{10}$$

Meanwhile, we can derive

$$\begin{aligned}&\left(\underbrace{\frac{P_{\mathrm{CPL1}}^{0}}{C_1 V_{\mathrm{bus1}}^{0}}\cdot g\left(x_{2n+1}\right)}_{\mathrm{CPL}}\underbrace{-\frac{1}{C_1 R_1}}_{\mathrm{CIL}}\right)\cdot x_{2n+1}\\&=\underbrace{-\frac{1}{C_1}\left(\frac{P_{\mathrm{CPL1}}^{0}}{v_{\mathrm{bus1}}}-\frac{P_{\mathrm{CPL1}}^{0}}{V_{\mathrm{bus1}}^{0}}\right)}_{\mathrm{CPL}}\underbrace{-\frac{1}{C_1 R_1}\left(v_{\mathrm{bus1}}-V_{\mathrm{bus1}}^{0}\right)}_{\mathrm{CIL}}\end{aligned}\tag{11}$$

where

$$g\left(x_{2n+1}\right)=\frac{1}{x_{2n+1}+V_{\mathrm{bus1}}^{0}}.\tag{12}$$

Similarly, we can find

$$\begin{cases}g\left(x_{2n+2}\right)=\frac{1}{x_{2n+2}+V_{\mathrm{bus2}}^{0}}\\\quad\vdots\\g\left(x_{3n}\right)=\frac{1}{x_{3n}+V_{\mathrm{bus}n}^{0}}.\end{cases}\tag{13}$$

It turns out to be a challenging task to conduct large signal Lyapunov stability with the $(3\times n)$th-order nonlinear dynamic system model of (2) since constructing the Lyapunov function will lead to a heavy computation burden. This will be the interest of the next section that proposes the T-S fuzzy modeling-based approach to simplify the large signal stability analysis of the DCMG cluster in the Lyapunov framework.

III. Proposed Approach Based on T-S Fuzzy Model for the DCMG Cluster

There are in general two ways to simplify Lyapunov-based stability analysis of nonlinear systems, i.e., reduced modeling of the original nonlinear system and simplifying the construction of Lyapunov function, and the T-S fuzzy multimodeling-based approach proposed in this article falls into the former one. The elegance of the T-S modeling approach is that the original nonlinear system can be approximated by a convex combination of a weighted set of linear models so that the problem with constructing Lyapunov functions is able to be reduced to a computation of a set of linear matrix inequalities (LMIs) [29].

Fig. 4 shows the flowchart of the large signal Lyapunov stability analysis based on the T-S fuzzy multimodeling approach for the DCMG cluster. There are two major parts, i.e., T-S fuzzy multimodeling and large signal stability analysis, covered with the proposed approach.

A. T-S Fuzzy Multimodeling for the DCMG Cluster

The T-S modeling uses a set of "if-then" fuzzy rules R^k for partitioning space into multiple small fuzzy regions where the nonlinear system can be represented by a set of linear models with weighted functions.

Rule R^k: If z_1 is ${F_1}^k$, … and z_q is ${F_q}^k$, the nonlinear system can be described as the subsystem:

$$\dot{\mathbf{x}}=A_k\cdot\mathbf{x}+B_k\cdot\mathbf{u}\tag{14}$$

where z_u $(u=1,2,\ldots,q)$ are functions of state variables, input variables, etc, and ${F_u}^k$ $(k=1,2,\ldots,r)$ denotes a fuzzy set or

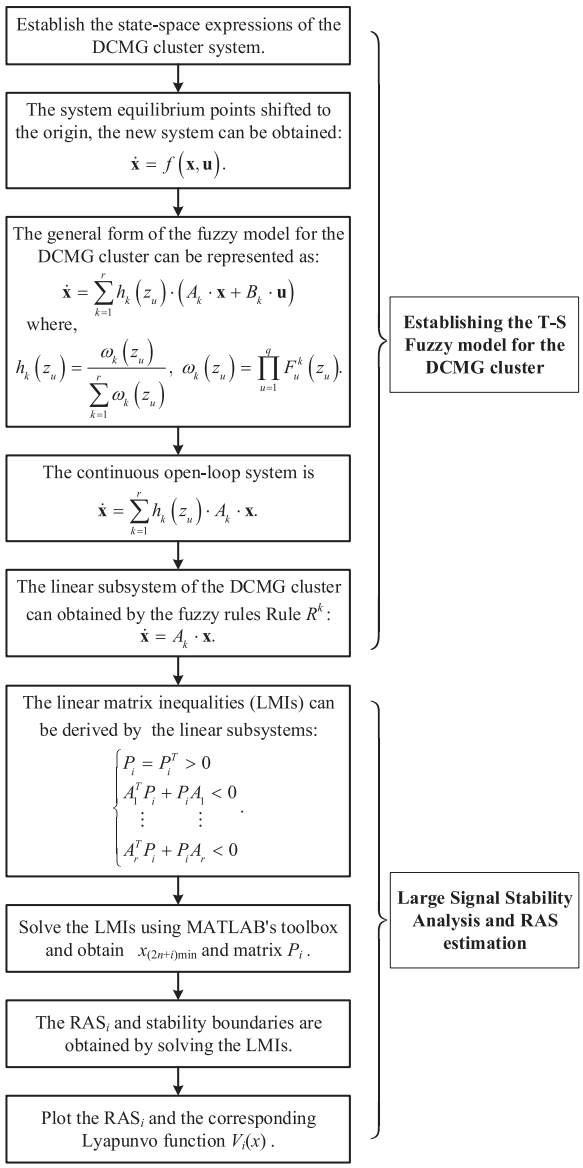

Fig. 4. Flowchart of Lyapunov stability analysis based on T-S fuzzy multimodeling approach.

so-called membership function and r is the number of fuzzy rules, respectively; and $A_k\in\mathbb{R}^{3n\times 3n}$, $B_k\in\mathbb{R}^{3n\times m}$, and $\mathbf{u}\in\mathbb{R}^{m\times 1}$stand for the dynamics matrix, the input matrix and the input (control) of the linear subsystems correspond to the fuzzy regions, respectively.

Then, the general form of the fuzzy model to represent the original nonlinear system is given by

$$\dot{\mathbf{x}}=\sum_{k=1}^{r}h_k\left(z_u\right)\cdot\left(A_k\cdot\mathbf{x}+B_k\cdot\mathbf{u}\right)\tag{15}$$

where $h_k(z_u)=\frac{\omega_k(z_u)}{\sum_{k=1}^{r}\omega_k(z_u)}$, $\omega_k(z_u)=\prod_{u=1}^{q}F_u^k(z_u)$, and $\sum_{k=1}^{r}h_k(z_u)=1$, respectively.

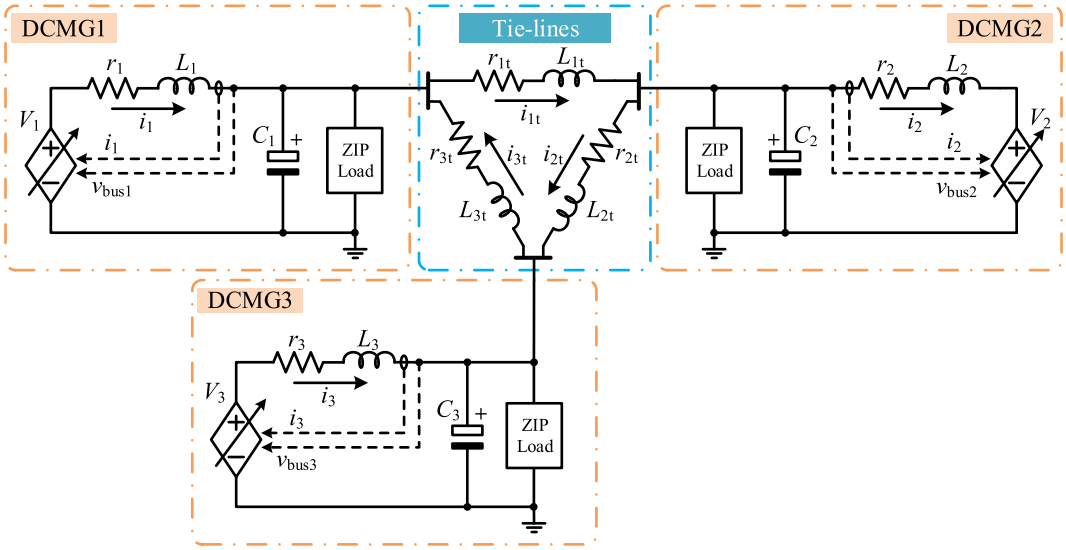

Fig. 5. Dynamic model of the studied DCMG cluster with three MGs.

B. Large Signal Stability Analysis of T-S Fuzzy Model

The DCMG cluster that guarantees Lyapunov stability is given by a set of the LMIs as

$$\begin{cases} P_i = P_i^T > 0 \\ A_1^T P_i + P_i A_1 < 0 \\ A_2^T P_i + P_i A_2 < 0 \\ \vdots \\ A_r^T P_i + P_i A_r < 0 \end{cases} \tag{16}$$

where P_i is a symmetric positive definite matrix, the subscript i denotes that P_i is related to the nonlinear parameter of the ith DCMG, and $r = 2^n$.

Theorem [30]–[33]: Consider the system as (15), if there exists a symmetric positive definite matrix P, $P \in \mathbb{R}^{3n\times 3n}$, satisfying

$$A_k^T P + P A_k < 0 \tag{17}$$

then the T-S fuzzy model is globally asymptotically stable.

Thus, the Lyapunov function ($V_i(x) = x^{\mathrm{T}} P_i x$) can be fully determined by solving the LMIs and calculating P_i according to the knowledge of the system model, viz., A_k in the LMIs.

To investigate the stability of the DCMG cluster, we focus on the variables that stand for the local bus voltage of each DCMG, i.e., $x_{2n+1}, x_{2n+2}, \ldots$, and x_{3n}. The LMI solver in the MATLAB toolbox can be deployed to calculate the minimum $x_{2n+1}, x_{2n+2}, \ldots$, and x_{3n}, i.e., $x_{(2n+1)\min}, x_{(2n+2)\min}, \ldots$, and $x_{(3n)\min}$, and solve the corresponding matrix P_i. Then, the RAS, e.g., the RAS_1, RAS_2, …, and RAS_n on x_1–x_{2n+1}, x_2–x_{2n+2}, …, and x_n–x_{3n} plane and corresponding Lyapunov function can be plotted out.

As such, the estimation of the RAS_1 on the x_1–x_{2n+1} plane, which corresponds to the phase plane of DCMG1 is given by (18) shown at the bottom of this page, where $x_1 = -P_{1(1,2n+1)} \cdot x_{(2n+1)\min}/P_{1(1,1)}$, $P_{1(1,2n+1)}$, and $P_{1(1,1)}$ are the element in row 1 and column $2n+1$ of the P_1 matrix, and the element in row 1 and column 1 of the P_1 matrix, respectively.

Similarly, the estimation of the RAS_i on the x_i–x_{2n+i} plane which corresponds to the phase plane of DCMGi is constrained by (19) shown at the bottom of the next page, where $x_i = -P_{i(i,2n+i)} \cdot x_{(2n+i)\min}/P_{i(i,i)}$, $i \le n$.

IV. Large Signal Stability Analysis

To exemplify the proposed approach, a DCMG cluster formed by interconnecting three DCMGs is considered as the case of study in this section. Fig. 5 shows the resultant complete equivalent circuit model of the DCMG cluster with three MGs.

A. Power Flow Analysis of the Steady-State Operation

Since the mechanism of the DCMG cluster system is unique from that of the single DCMG. It is necessary to point out the power flows of the DCMG cluster in the steady-state operation before we embark on its dynamic characteristics. The power flow among these three DCMGs is determined by their local bus voltages, which is usually achieved by the tertiary level control.

The power flow of the DCMG cluster is illustrated in Fig. 6 by the output characteristics (*V-I* droop curves) of each DCMG

$$\begin{cases} V_1(x) = P_{1(1,1)}x_1^2 + P_{1(1,2n+1)} + P_{1(2n+1,1)}x_1 x_{2n+1} + P_{1(2n+1,2n+1)}x_{2n+1}^2 \\ \mathrm{RAS}_1 = \left\{ x : V_1(x) \le V_{1\min}\left(x_1, \underbrace{0,\ldots,0}_{n-1}\underbrace{0,\ldots,0}_{n} x_{(2n+1)\min}, \underbrace{0,\ldots,0}_{n-1} \right) \right\} \end{cases} \tag{18}$$

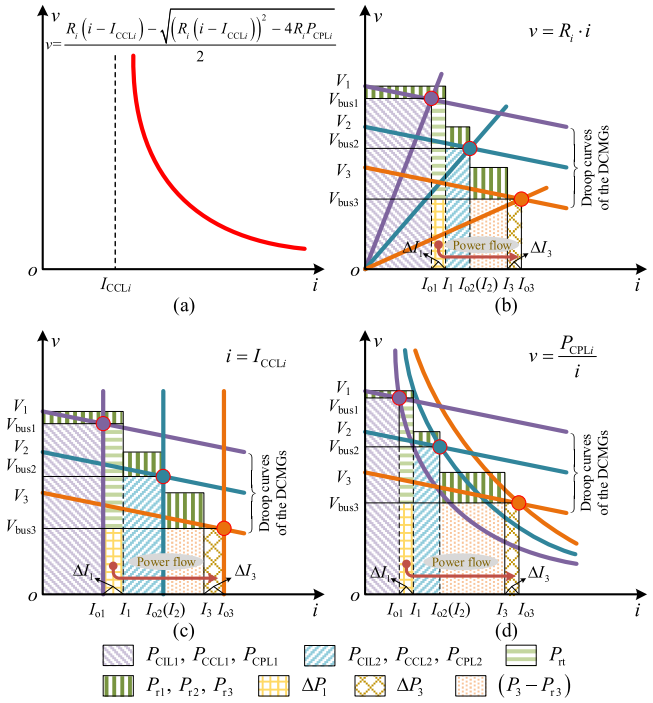

Fig. 6. *V-I* curve of the ZIP load and illustration of the power flow in the DCMG cluster by the characteristics of the CIL, CCL, and CPL, respectively. (a) ZIP load. (b) CIL. (c) CCL. (d) CPL.

with the CIL, CCL, and CPL, respectively. Since the product of voltage and current stands for the power, the shaded squares represent the power within each DCMG. The power or current will be always flowing from the DCMG with power surplus (higher bus voltage) to the DCMG with power deficiency (lower bus voltage) through the tie-line.

As shown in Fig. 6, the order of the state-of-charge (SoC) of the three DCMGs is DCMG1 highest, DCMG2 medium, and DCMG3 lowest. We assume in this case that DCMG2 can maintain the power balance between source and load side, while the power flow will only happen between DCMG1 and DCMG3.

Taking Fig. 6(b) as an example, the load power for DCMG1 can be expressed by

$$P_{\mathrm{CIL1}} = P_1 - P_{r1} - P_{rt} - \Delta P_1 \tag{20}$$

where P_{CIL1}, P_1, P_{r1}, P_{rt}, and ΔP_1 represent the power of CIL1, the power provided by DCMG1, the loss of power on lines in DCMG1, the loss of power on tie-lines, and the power flowing to the other DCMG, respectively.

TABLE I
PARAMETERS OF THE DCMG CLUSTER MODEL

	Parameters	Value
Single DCMG	V_{bus1}, V_{bus2}, V_{bus3}	48.5 V, 48.0 V, 47.5 V
	r_i (i = 1,2,3)	0.2 Ω
	L_i (i = 1,2,3)	500 μH
	C_i (i = 1,2,3)	3000 μF
	$P_{\mathrm{CPL}i}$ (i = 1,2,3)	2 kW
	R_i (i = 1,2,3)	100 Ω
	$I_{\mathrm{CCL}i}$ (i = 1,2,3)	10 A
Tie-lines	$r_{1\mathrm{t}}$	0.2 Ω
	$r_{2\mathrm{t}}$	0.4 Ω
	$r_{3\mathrm{t}}$	0.8 Ω
	$L_{1\mathrm{t}}$	50 μH
	$L_{2\mathrm{t}}$	100 μH
	$L_{3\mathrm{t}}$	200 μH

As such, the load power of DCMG3 and the power needs to be supplied by the DCMG1 can be expressed by

$$P_{\mathrm{CIL3}} = P_3 - P_{r3} + \Delta P_3 \tag{21}$$

where P_{CIL3}, P_3, P_{r3}, and ΔP_3 denote the power of CIL3, the power provided by DCMG3, the loss of power on lines in DCMG3, and the power from DCMG1, respectively.

It should be noted that $\Delta P_1 = \Delta P_3$ in Fig. 6(b), which stands for the power exchange between DCMG1 and DCMG3 in this case. Meanwhile, DCMG2 can maintain the power balance itself, which is given by

$$P_{\mathrm{CIL2}} = P_2 - P_{r2} \tag{22}$$

where P_{CIL2}, P_2, and P_{r2} represent the power of CIL2, the power provided by DCMG2, and the loss of power on lines in DCMG2, respectively.

Similar to the power flow case in the DCMG cluster with the CIL as shown in Fig. 6(b), the CCL in Fig. 6(c), and CPL in Fig. 6(d) has the same power flow scenario and the equations as with (20), (21), and (22).

B. Large Signal Lyapunov Stability Analysis

As in Fig. 5, and thus $n = 3$, $r = 8$, and we go through the fuzzy rules, i.e., Rule R^k ($k = 1, 2, \ldots, r$), and solve the matrices A_k of the local linearized subsystem, and the normalized weight functions $h_k(z_u)$ in Appendix A.

Given the parameters in Table I for the dynamic model of the DCMG cluster in Fig. 5, the LMI solver calculates

$$\begin{cases} V_i(x) = P_{i(i,i)}x_i^2 + P_{i(i,2n+i)} + P_{i(2n+i,i)}x_i x_{2n+i} + P_{i(2n+i,2n+i)}x_{2n+i}^2 \\ \mathrm{RAS}_i = \{x : V_i(x) \le V_{i\min}(x)\} \\ V_{i\min}(x) = V_{i\min}\left(\underbrace{0,\ldots,0}_{i-1}, x_i, \underbrace{0,\ldots,0}_{n-i}\underbrace{0,\ldots,0}_{n}\underbrace{0,\ldots,0}_{i-1}x_{(2n+i)\min}, \underbrace{0,\ldots,0}_{n-i}\right) \end{cases} \tag{19}$$

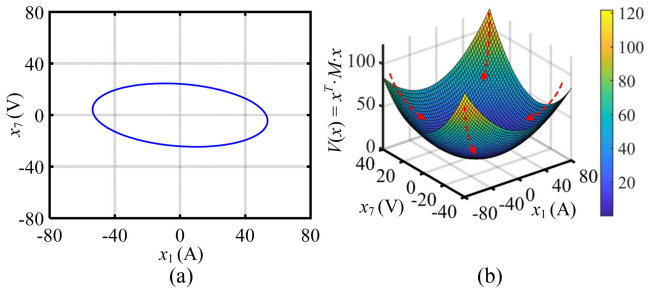

Fig. 7. Illustration of the RAS_1 on the x_1-x_7 plane and the Lyapunov function. (a) RAS_1 on the x_1-x_7 plane. (b) Illustration of the constructed Lyapunov function.

TABLE II
STABILITY BOUNDARIES OF L_i, C_i, AND $P_{\mathrm{CPL}i}$ PARAMETERS

Parameters	Stability Boundaries
L_i (i = 1,2,3)	$\leq$ 699 μH
C_i (i = 1,2,3)	$\geq$ 2146 μF
$P_{\mathrm{CPL}i}$ (i = 1,2,3)	$\leq$ 2788 W

$x_{7\min} = -24.6$, $x_{8\min} = -24.2$, $x_{9\min} = -23.1$, and the corresponding matrix P_i which is detailed in Appendix B.

The estimations of RAS_1, RAS_2, and RAS_3 are given by

$$\begin{cases} \mathrm{RAS}_1 : V_1(x) = 0.0074x_1^2 + 0.0058x_1x_7 \\ \quad +0.0351x_7^2 \leq 20.5520 \\ \mathrm{RAS}_2 : V_2(x) = 0.0095x_2^2 + 0.0074x_2x_8 \\ \quad +0.0439x_8^2 \leq 24.8349 \\ \mathrm{RAS}_3 : V_3(x) = 0.0094x_3^2 + 0.0074x_3x_9 \\ \quad +0.0452x_9^2 \leq 23.3398. \end{cases} \tag{23}$$

For simplicity, DCMG1 is picked to look at the estimated RAS. Fig. 7 shows the estimated results where the RAS, viz. the stable region, is shown in Fig. 7(a), and the constructed Lyapunov function $V(x)$ with the positive definite value in Fig. 7(b) supports the results. In other words, the system is asymptotically stable subject to large signal disturbances within the RAS about the equilibrium point.

The boundaries of CPLs (P_{CPL1}, P_{CPL2}, and P_{CPL3} have step transient independently), which can guarantee the stability of the system are obtained as $P_{\mathrm{CPL1}} \leq 3260$ W, $P_{\mathrm{CPL2}} \leq 3242$ W, and $P_{\mathrm{CPL3}} \leq 3157$ W.

The stability boundaries of these parameters (L_i, C_i, and $P_{\mathrm{CPL}i}$), are listed in Table II with the other parameters determined as listed in Table I, assuming that parameters of the same type remain consistent for the three DCMGs.

Based on the RAS estimation technique, three scenarios, i.e., change of the parameters of the reduced circuit model, change of power flows among the interconnected DCMGs, and variation of the DCMG cluster topology will be considered in the large signal stability analysis of the DCMG cluster system.

1) Change of the Parameters of the DCMG Cluster Model: Fig. 8 shows the evolution of the RASs with changes of a set of parameters, including the bus capacitance in Fig. 8(a), the line inductance in each DCMG in Fig. 8(b), the line resistance in each DCMG in Fig. 8(c), the CPL in Fig. 8(d), the CIL in Fig. 8(e), and the inductance of the tie-lines in Fig. 8(f), respectively. It suggests that the increase of the bus capacitance and line resistance in each DCMG will significantly enlarge the RAS, whereas the increase of the line inductance and the CPL will have a negative impact on the stability region. Moreover, the CIL in parallel will have a positive impact on the RAS, and the inductance of the tie-line has little effect on the RAS.

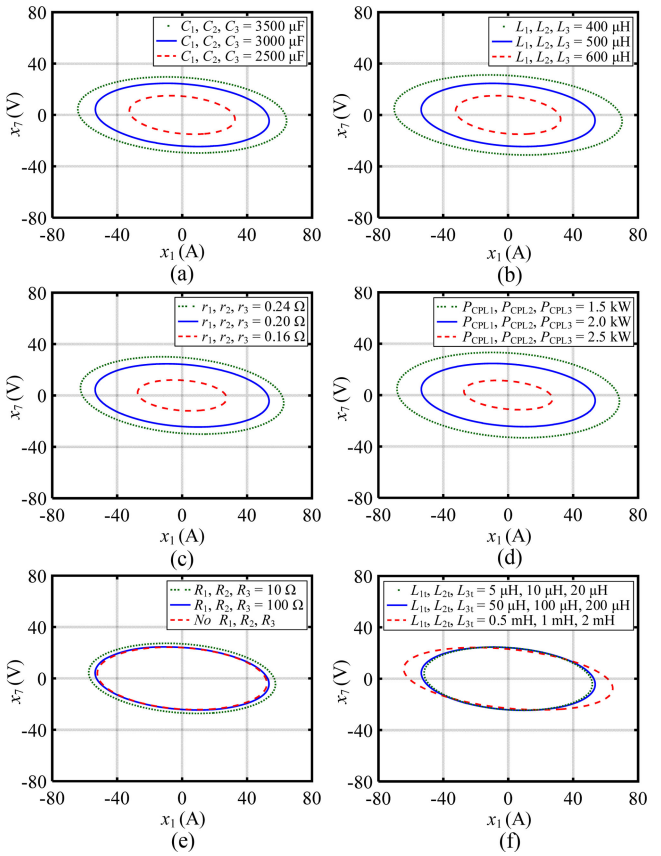

Fig. 8. Evolution of estimated RASs with changes of the circuit parameters on the x_1-x_7 plane. (a) Bus capacitance. (b) Equivalent line inductance in single DCMG. (c) Equivalent line resistance in single DCMG. (d) CPL. (e) CIL. (f) Equivalent inductance of the tie-lines.

TABLE III
LOCAL DC BUS VOLTAGE FOR STUDY CASES

Study Cases	V_{bus1}	V_{bus2}	V_{bus3}
Case I	50.4 V	48.0 V	45.6 V
Case II	50.4 V	45.6 V	45.6 V
Case III	50.4 V	50.4 V	45.6 V

2) Change of Power Flow: In this scenario, the power flow among the DCMGs in the cluster could be changed subject to load conditions or network operations. Table III lists the local bus voltage with three cases considered, and Fig. 9 depicts the study cases with changes of power flow in the DCMG cluster system, from which DCMG1 provides power to DCMG2 and DCMG3, and DCMG2 outputs power to DCMG3 in Fig. 9(a) since the local bus voltages indicate that DCMG1 is at highest

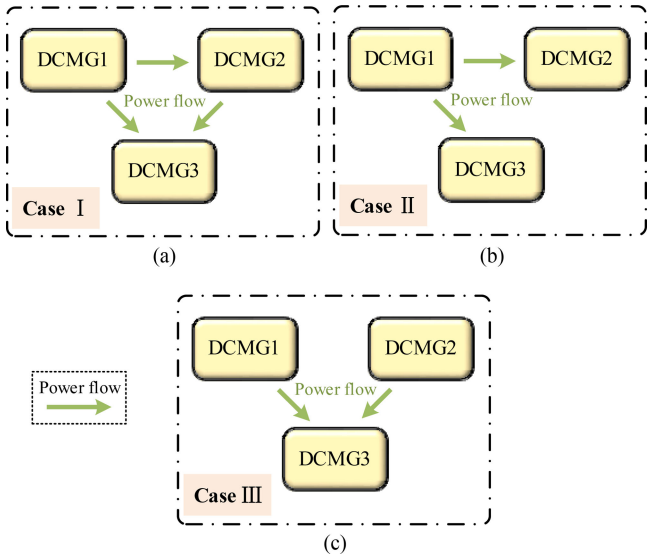

Fig. 9. Illustration of power flows among DCMGs. (a) Power flows among the three DCMGs. (b) DCMG1 provides power flows to DCMG2 and DCMG3. (c) Both DCMG1 and DCMG2 provide power to DCMG3.

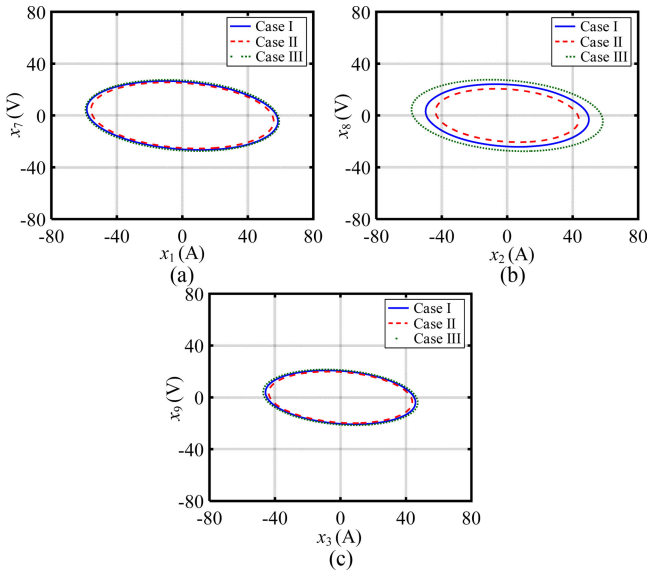

Fig. 10. Estimated RASs for study cases. (a) RASs on the x_1-x_7 plane. (b) RASs on the x_2-x_8 plane. (c) RASs on the x_3-x_9 plane.

SoC, while DCMG2 at middle SoC, and DCMG3 at lowest. Similarly, DCMG1 provides power to both DCMG2 and DCMG3 in Fig. 9(b), and both DCMG1 and DCMG2 provide power to DCMG3 in Fig. 9(c), respectively.

The estimated RAS on the x_1-x_7, x_2-x_8, and x_3-x_9 plane with the three cases are shown in Fig. 10(a), (b), and (c), respectively. It can be seen that although Case III achieves maximum RAS, Case II smallest RAS, and Case I medium RAS for all the DCMGs, the change of power flow does not have a significant influence on the RAS. Interestingly, it can be found that the DCMG1, which always provides power to the external has the

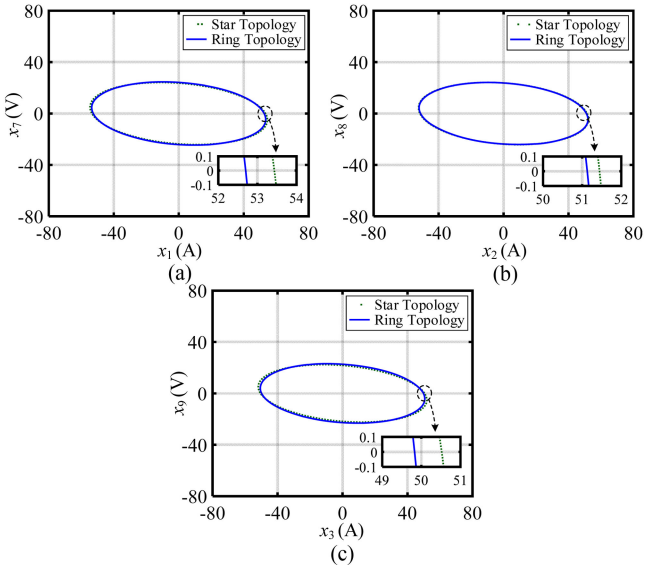

Fig. 11. Estimated RAS for the topology change of the DCMG cluster from the ring to the star interconnection. (a) RASs on the x_1-x_7 plane. (b) RASs on the x_2-x_8 plane. (c) RASs on the x_3-x_9 plane.

largest RAS in Fig. 10(a), while the DCMG3 which receives power from other grids has the smallest RAS in Fig. 10(c).

3) Change of the DCMG Cluster Topology: This scenario is intended to observe the influence of the variation of the DCMG cluster topology on the stability region. As aforementioned, the DCMG cluster in this article is of a ring topology, i.e., the three DCMGs are interconnected as a ring network, even it can also be a star topology.

It is assumed that #3 tie-line in Fig. 5 will be disconnected to make the change of the DCMG cluster topology from the ring to the star interconnection. In this scenario, the equivalent circuit model of the DCMG cluster in Fig. 5 will be reduced to the eighth-order dynamic system of the star topology from the original ninth-order one of the ring topology. The estimated RAS with the topological change is shown in Fig. 11 where the RAS with local voltage and current of DCMG1, DCMG2, and DCMG3 are given in Fig. 11(a), (b), and (c), respectively. One can see that the variation of the DCMG cluster topology from the ring to the star interconnection has little impact on the large signal stability of the system. In other words, the ring topology is the one with high reliability and redundancy in terms of the stability region.

V. Simulations and Experiments

A. Simulation Results

To validate the analysis, a simulation model was built in MATLAB/Simulink environment, and the parameters are in consistent with the large signal stability analysis in Section IV.

Fig. 12 shows the transient response to the CPL step from 2 to 3.35 kW, and the oscillation appears due to the stable boundary for the CPL is solved based on the LMIs in the last section as $P_{\mathrm{CPL1}} \leq 3.26$ kW. Meanwhile, the phase trajectory of the DCMG1 in the cluster with the CPL step disturbance is

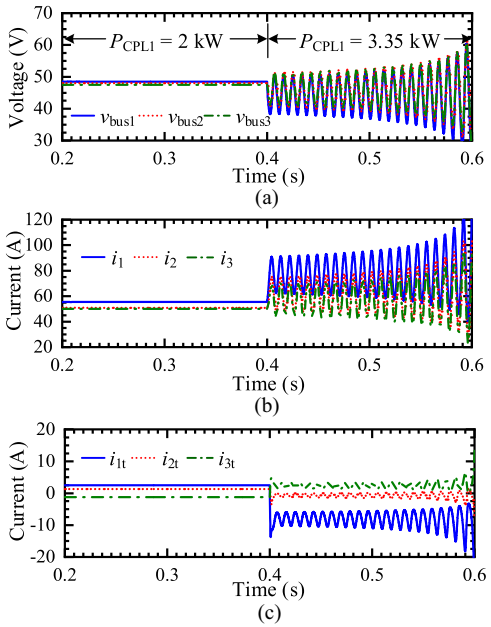

Fig. 12. Simulation results with CPL step transient. (a) DC bus voltage. (b) Equivalent line inductor current. (c) Tie-line current.

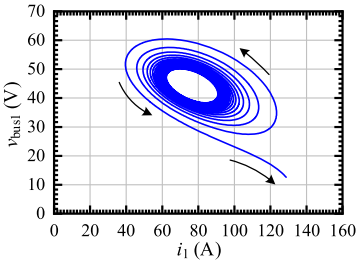

Fig. 13. Phase trajectory ($x_1 - x_7$ plane) of the CPL step response.

illustrated in Fig. 13 where the system ends with divergence after the transient. The simulation agrees well with the large signal stability analysis with the T-S multimodeling approach.

Fig. 14 shows the simulated response to the change of power flows among the three DCMGs in the cluster. It can be seen that the DCMG cluster starts with the case I, and is switched to case II at 0.4 s, and transitioned to case III at 0.6 s, and the smooth transition demonstrates that the power flow can hardly impact the stability of the system.

Fig. 15 shows the simulation results for the change of the DCMG cluster topology from the ring to the star interconnection. With the disconnection of the #3 tie-line at 0.5 s, the DCMG cluster makes the smooth transition of the topological change thanks to the subtle difference between the ring and star topologies in terms of the RAS. It also implies that the ring topology of the DCMG cluster is capable of achieving high continuity and resilience of the power supply.

B. Experimental Results

To further verify the large signal stability analysis method of the DCMG cluster based on T-S multimodeling, the hardware

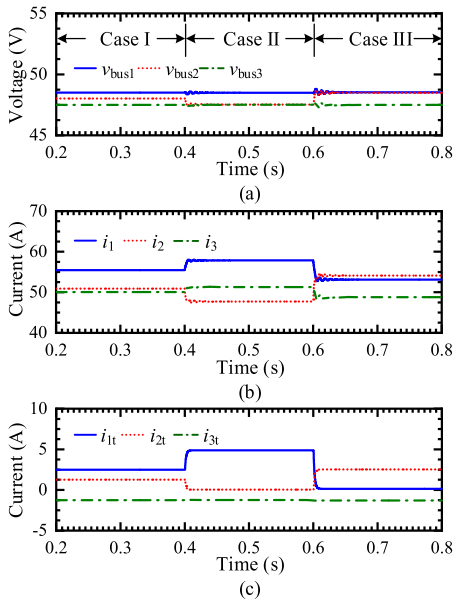

Fig. 14. Simulation results for the change of power flow. (a) DC bus voltage. (b) Equivalent line inductor current. (c) Tie-line current.

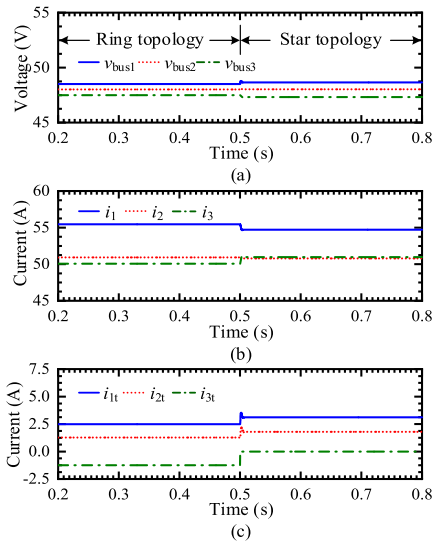

Fig. 15. Simulation results for the topological change with #3 tie-line disconnected. (a) DC bus voltage. (b) Equivalent line inductor current. (c) Tie-line current.

test results are given in addition to the simulations. A scaled-down laboratory prototype with its parameters shown in Table IV is built for experimental verification. The tie-line parameters are considered to be consistent for simplification. The load model of DCMG1 is CIL and CPL in parallel, and the load model of DCMG2 and DCMG3 is CPL for the laboratory prototype. The large signal stability boundary for CPL1 is $P_{\mathrm{CPL1}} \leq 196$ W which is obtained by the above method.

Fig. 16 shows experimental results of the transient response to the CPL step change, which agrees well with the stability boundary. Fig. 16(a) shows that the system in ring topology can gradually converge and stabilize at the new operating point when the CPL1 is changed from 100 to 180 W. The transient responses

TABLE IV
EXPERIMENTAL PARAMETERS OF THE DCMG CLUSTER

	Parameters	Value
Single DCMG	V_{bus1}, V_{bus2}, V_{bus3}	48.2 V, 48.0 V, 47.8 V
	r_i (i = 1,2,3)	0.2 Ω
	L_i (i = 1,2,3)	300 μH
	C_i (i = 1,2,3)	85 μF
	P_{CPLi} (i = 1,2,3)	100 W
	R_i (i = 1)	300 Ω
Tie-lines	r_{it} (i = 1,2,3)	0.4 Ω
	L_{it} (i = 1,2,3)	100 μH

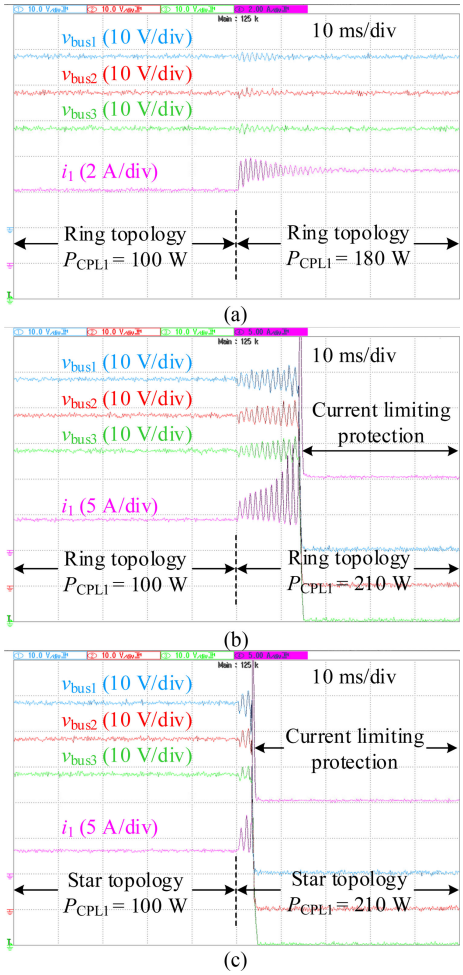

Fig. 16. Experimental results of the response to the CPL step change. (a) CPL1 changed from 100 to 180 W in the ring topology. (b) CPL1 changed from 100 to 210 W in the ring topology. (c) CPL1 changed from 100 to 210 W in the star topology.

of the ring and star topology in Fig. 16(b) and (c), respectively, show that the load step contributes to the instabilities of the system in these conditions.

Fig. 17 shows the experimental results of the response to the change of the power flow in the DCMG cluster, which is

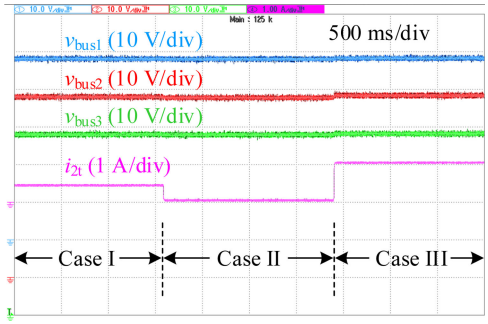

Fig. 17. Experimental results of the response to the change of power flow.

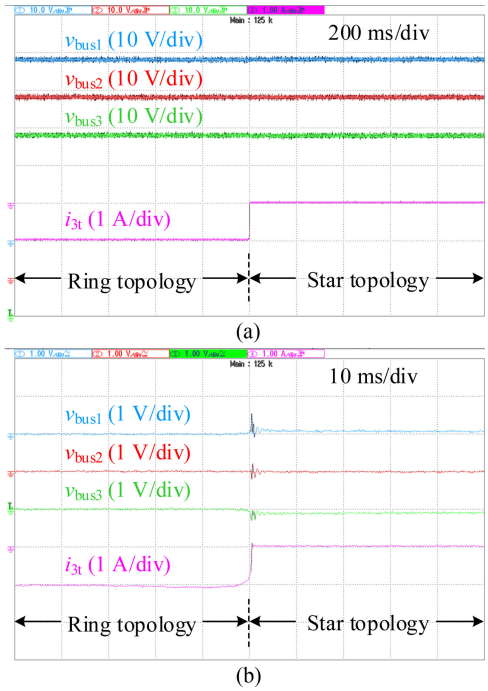

Fig. 18. Experimental results of the response to the topology change. (a) Transient response from ring to star topology. (b) Zoom-in view of the response.

consistent with the simulations that suggest smooth transitions among case I, case II, and case III.

Fig. 18 shows the experimental results of the response to the topology change of the DCMG cluster from the ring to the star interconnection via the disconnection of the #3 tie-line, and the zoom-in view of the response suggests that the transient has nearly zero impact on the stability of the system.

In a word, all the experimental results have verified the analysis along with the simulations.

VI. CONCLUSION

This article proposes a general, simple yet effective approach for large signal stability analysis based on T-S multimodeling for the DCMG cluster. With the proposed approach, the nonlinear higher-order dynamic model of the DCMG cluster can be approximated by the convex combination of a set of linear models, and thus the large signal Lyapunov stability analysis

of the system has been reduced to solving the LMIs, which is accessible by the standard LMI tools. Besides, RAS, viz., the stability region of the system has also been estimated, and the time-domain simulations and experimental results have demonstrated the effectiveness of the estimations. Conclusions can be drawn as follows.

1) The increase of the bus capacitance will improve the large signal stability of the DCMG cluster, whereas the CPL and the equivalent inductance of each DCMG will deteriorate the stability, and the required value of these components for satisfying the stability boundary can be solved by the given RAS. In addition, the CIL in parallel will improve the stability and the smaller resistance of the CIL has the better stability. However, the inductance of the tie-line has little effect on the stability of the DCMG cluster.
2) The estimation of the RAS is effective in predicting the large signal stable region of the DCMG cluster subject to the disturbances, i.e., change of the CPL, power flow, and the topology.
3) The transition from the ring topology to the star one of the DCMG cluster can remain the large signal stability region, which says the high redundancy and resilience of the ring topology of the network.

APPENDIX

A. Fuzzy Rules and Solution of Linear Subsystems

With $n = 3$, $k = 1, \ldots, 8$, noting that $g(x_7)$, $g(x_8)$, and $g(x_9)$ are nonlinear elements in the system (14), the original nonlinear dynamic system model of the DCMG cluster can be linearized locally based on the partition of the original state matrix which is written as

$$\dot{\mathbf{x}} = A_k \cdot \mathbf{x} = \left[\begin{array}{c|c|c} A_{k-1} & O_{n\times n} & A_{k-2} \\ \hline O_{n\times n} & A_{k-3} & A_{k-4} \\ \hline A_{k-5} & A_{k-6} & A_{k-7} \end{array}\right] \cdot \mathbf{x} \tag{24-a}$$

where the block matrices $A_{k\_a}(a = 1, \cdots, 7) \in \mathbb{R}^{3\times 3}$, in solving the local linearized subsystem, $A_{k\_a}(a = 1, \cdots, 6)$ is invariant, while the matrix A_{k_7} can be given as (24-b).

Fuzzy rules are primarily determined by $g(x_7)$, $g(x_8)$, and $g(x_9)$ in (15) as follows according to the boundary values of the bus voltages of the three DCMGs.

Rule R^1: If x_7, x_8, and x_9 reaches $x_{7\max}$, $x_{8\min}$, and $x_{9\min}$, respectively, then the linear subsystem can be derived as

$$\dot{\mathbf{x}} = A_1 \cdot \mathbf{x} = \left[\begin{array}{c|c|c} A_{k-1} & O_{n\times n} & A_{k-2} \\ \hline O_{n\times n} & A_{k-3} & A_{k-4} \\ \hline A_{k-5} & A_{k-6} & A_{1-7} \end{array}\right] \cdot \mathbf{x} \tag{25-a}$$

where

$$\begin{cases} g(x_7) = g(x_7)_{\min} = \frac{1}{x_{7\max} + V^0_{\text{bus1}}} \\ g(x_8) = g(x_8)_{\max} = \frac{1}{x_{8\min} + V^0_{\text{bus2}}} \\ g(x_9) = g(x_9)_{\max} = \frac{1}{x_{9\min} + V^0_{\text{bus3}}}. \end{cases}$$

Rule R^2: If x_7, x_8, and x_9 reaches $x_{7\min}$, $x_{8\min}$, and $x_{9\min}$, respectively, then the linear subsystem can be derived as

$$\dot{\mathbf{x}} = A_2 \cdot \mathbf{x} = \left[\begin{array}{c|c|c} A_{k-1} & O_{n\times n} & A_{k-2} \\ \hline O_{n\times n} & A_{k-3} & A_{k-4} \\ \hline A_{k-5} & A_{k-6} & A_{2-7} \end{array}\right] \cdot \mathbf{x} \tag{25-b}$$

where

$$\begin{cases} g(x_7) = g(x_7)_{\max} = \frac{1}{x_{7\min} + V^0_{\text{bus1}}} \\ g(x_8) = g(x_8)_{\max} = \frac{1}{x_{8\min} + V^0_{\text{bus2}}} \\ g(x_9) = g(x_9)_{\max} = \frac{1}{x_{9\min} + V^0_{\text{bus3}}}. \end{cases}$$

Rule R^3: If x_7, x_8, and x_9 reaches $x_{7\max}$, $x_{8\max}$, and $x_{9\min}$, respectively, then the linear subsystem can be derived as

$$\dot{\mathbf{x}} = A_3 \cdot \mathbf{x} = \left[\begin{array}{c|c|c} A_{k-1} & O_{n\times n} & A_{k-2} \\ \hline O_{n\times n} & A_{k-3} & A_{k-4} \\ \hline A_{k-5} & A_{k-6} & A_{3-7} \end{array}\right] \cdot \mathbf{x} \tag{25-c}$$

where

$$\begin{cases} g(x_7) = g(x_7)_{\min} = \frac{1}{x_{7\max} + V^0_{\text{bus1}}} \\ g(x_8) = g(x_8)_{\min} = \frac{1}{x_{8\max} + V^0_{\text{bus2}}} \\ g(x_9) = g(x_9)_{\max} = \frac{1}{x_{9\min} + V^0_{\text{bus3}}}. \end{cases}$$

Rule R^4: If x_7, x_8, and x_9 reaches $x_{7\max}$, $x_{8\min}$, and $x_{9\max}$, respectively, then the linear subsystem can be derived as

$$\dot{\mathbf{x}} = A_4 \cdot \mathbf{x} = \left[\begin{array}{c|c|c} A_{k-1} & O_{n\times n} & A_{k-2} \\ \hline O_{n\times n} & A_{k-3} & A_{k-4} \\ \hline A_{k-5} & A_{k-6} & A_{4-7} \end{array}\right] \cdot \mathbf{x} \tag{25-d}$$

where

$$\begin{cases} g(x_7) = g(x_7)_{\min} = \frac{1}{x_{7\max} + V^0_{\text{bus1}}} \\ g(x_8) = g(x_8)_{\max} = \frac{1}{x_{8\min} + V^0_{\text{bus2}}} \\ g(x_9) = g(x_9)_{\min} = \frac{1}{x_{9\max} + V^0_{\text{bus3}}}. \end{cases}$$

Rule R^5: If x_7, x_8, and x_9 reaches $x_{7\min}$, $x_{8\max}$, and $x_{9\min}$, respectively, then the linear subsystem can be derived as

$$\dot{\mathbf{x}} = A_5 \cdot \mathbf{x} = \left[\begin{array}{c|c|c} A_{k-1} & O_{n\times n} & A_{k-2} \\ \hline O_{n\times n} & A_{k-3} & A_{k-4} \\ \hline A_{k-5} & A_{k-6} & A_{5-7} \end{array}\right] \cdot \mathbf{x} \tag{25-e}$$

where

$$\begin{cases} g(x_7) = g(x_7)_{\max} = \frac{1}{x_{7\min} + V^0_{\text{bus1}}} \\ g(x_8) = g(x_8)_{\min} = \frac{1}{x_{8\max} + V^0_{\text{bus2}}} \\ g(x_9) = g(x_9)_{\max} = \frac{1}{x_{9\min} + V^0_{\text{bus3}}}. \end{cases}$$

$$A_{k\_7} = \begin{bmatrix} \frac{P^0_{\text{CPL1}}}{C_1 V^0_{\text{bus1}}} \cdot g(x_7) - \frac{1}{C_1 R_1} & 0 & 0 \\ 0 & \frac{P^0_{\text{CPL2}}}{C_2 V^0_{\text{bus2}}} \cdot g(x_8) - \frac{1}{C_2 R_2} & 0 \\ 0 & 0 & \frac{P^0_{\text{CPL3}}}{C_3 V^0_{\text{bus3}}} \cdot g(x_9) - \frac{1}{C_3 R_3} \end{bmatrix} \tag{24-b}$$

Rule R^6: If x_7, x_8, and x_9 reaches $x_{7\min}$, $x_{8\min}$, and $x_{9\max}$, respectively, then the linear subsystem can be derived as

$$\dot{\mathbf{x}} = A_6 \cdot \mathbf{x} = \left[\begin{array}{c|c|c} A_{k-1} & O_{n\times n} & A_{k-2} \\ \hline O_{n\times n} & A_{k-3} & A_{k-4} \\ \hline A_{k-5} & A_{k-6} & A_{6-7} \end{array}\right] \cdot \mathbf{x} \tag{25-f}$$

where

$$\begin{cases} g(x_7) = g(x_7)_{\max} = \frac{1}{x_{7\min}+V^0_{\text{bus1}}} \\ g(x_8) = g(x_8)_{\max} = \frac{1}{x_{8\min}+V^0_{\text{bus2}}} \\ g(x_9) = g(x_9)_{\min} = \frac{1}{x_{9\max}+V^0_{\text{bus3}}}. \end{cases}$$

Rule R^7: If x_7, x_8, and x_9 reaches $x_{7\max}$, $x_{8\max}$, and $x_{9\max}$, respectively, then the linear subsystem can be derived as

$$\dot{\mathbf{x}} = A_7 \cdot \mathbf{x} = \left[\begin{array}{c|c|c} A_{k-1} & O_{n\times n} & A_{k-2} \\ \hline O_{n\times n} & A_{k-3} & A_{k-4} \\ \hline A_{k-5} & A_{k-6} & A_{7-7} \end{array}\right] \cdot \mathbf{x} \tag{25-g}$$

where

$$\begin{cases} g(x_7) = g(x_7)_{\min} = \frac{1}{x_{7\max}+V^0_{\text{bus1}}} \\ g(x_8) = g(x_8)_{\min} = \frac{1}{x_{8\max}+V^0_{\text{bus2}}} \\ g(x_9) = g(x_9)_{\min} = \frac{1}{x_{9\max}+V^0_{\text{bus3}}}. \end{cases}$$

Rule R^8: If x_7, x_8, and x_9 reaches $x_{7\min}$, $x_{8\max}$, and $x_{9\max}$, respectively, then the linear subsystem can be derived as

$$\dot{\mathbf{x}} = A_8 \cdot \mathbf{x} = \left[\begin{array}{c|c|c} A_{k-1} & O_{n\times n} & A_{k-2} \\ \hline O_{n\times n} & A_{k-3} & A_{k-4} \\ \hline A_{k-5} & A_{k-6} & A_{8-7} \end{array}\right] \cdot \mathbf{x} \tag{25-h}$$

where

$$\begin{cases} g(x_7) = g(x_7)_{\max} = \frac{1}{x_{7\min}+V^0_{\text{bus1}}} \\ g(x_8) = g(x_8)_{\min} = \frac{1}{x_{8\max}+V^0_{\text{bus2}}} \\ g(x_9) = g(x_9)_{\min} = \frac{1}{x_{9\max}+V^0_{\text{bus3}}}. \end{cases}$$

Hence, the normalized weight functions are determined according to fuzzy rules:

$$\begin{cases} h_1 = \omega_1 = \frac{z_1-x_{7\min}}{x_{7\max}-x_{7\min}} \cdot \frac{-z_2+x_{8\max}}{x_{8\max}-x_{8\min}} \cdot \frac{-z_3+x_{9\max}}{x_{9\max}-x_{9\min}} \\ h_2 = \omega_2 = \frac{-z_1+x_{7\max}}{x_{7\max}-x_{7\min}} \cdot \frac{-z_2+x_{8\max}}{x_{8\max}-x_{8\min}} \cdot \frac{-z_3+x_{9\max}}{x_{9\max}-x_{9\min}} \\ h_3 = \omega_3 = \frac{z_1-x_{7\min}}{x_{7\max}-x_{7\min}} \cdot \frac{z_2-x_{8\min}}{x_{8\max}-x_{8\min}} \cdot \frac{-z_3+x_{9\max}}{x_{9\max}-x_{9\min}} \\ h_4 = \omega_4 = \frac{z_1-x_{7\min}}{x_{7\max}-x_{7\min}} \cdot \frac{-z_2+x_{8\max}}{x_{8\max}-x_{8\min}} \cdot \frac{z_3-x_{9\min}}{x_{9\max}-x_{9\min}} \\ h_5 = \omega_5 = \frac{-z_1+x_{7\max}}{x_{7\max}-x_{7\min}} \cdot \frac{z_2-x_{8\min}}{x_{8\max}-x_{8\min}} \cdot \frac{-z_3+x_{9\max}}{x_{9\max}-x_{9\min}} \\ h_6 = \omega_6 = \frac{-z_1+x_{7\max}}{x_{7\max}-x_{7\min}} \cdot \frac{-z_2+x_{8\max}}{x_{8\max}-x_{8\min}} \cdot \frac{z_3-x_{9\min}}{x_{9\max}-x_{9\min}} \\ h_7 = \omega_7 = \frac{z_1-x_{7\min}}{x_{7\max}-x_{7\min}} \cdot \frac{z_2-x_{8\min}}{x_{8\max}-x_{8\min}} \cdot \frac{z_3-x_{9\min}}{x_{9\max}-x_{9\min}} \\ h_8 = \omega_8 = \frac{-z_1+x_{7\max}}{x_{7\max}-x_{7\min}} \cdot \frac{z_2-x_{8\min}}{x_{8\max}-x_{8\min}} \cdot \frac{z_3-x_{9\min}}{x_{9\max}-x_{9\min}} \end{cases} \tag{26}$$

where $z_1 = x_7$, $z_2 = x_8$, and $z_3 = x_9$.

B. Results of the Matrix P_i

In Section IV-B, the matrix P_i can be obtained by solving the LMIs using MATLAB's LMI toolbox.

The matrix P_1 corresponding to the RAS1 of the DCMG1, P_2 corresponding to the RAS2 of the DCMG2, and P_3 corresponding to the RAS3 of the DCMG3 are solved as (27), (28), and (29) shown at the bottom of this page, respectively.

$$P_1 = \begin{bmatrix} 0.0074 & 1.4575\times10^{-4} & 7.1200\times10^{-4} & 1.1596\times10^{-4} & 6.8806\times10^{-5} & -4.0446\times10^{-5} & 0.0029 & 0.0038 & 0.0046 \\ 1.4575\times10^{-4} & 0.0076 & 2.1839\times10^{-4} & -1.1476\times10^{-4} & 3.7586\times10^{-5} & -9.4411\times10^{-6} & 0.0031 & 0.0024 & 0.0036 \\ 7.1200\times10^{-4} & 2.1839\times10^{-4} & 0.0069 & -5.6191\times10^{-5} & -1.3438\times10^{-4} & 7.3451\times10^{-5} & 0.0031 & 0.0033 & 0.0016 \\ 1.1596\times10^{-4} & -1.1476\times10^{-4} & -5.6191\times10^{-5} & 4.6186\times10^{-4} & -5.9539\times10^{-5} & 3.5526\times10^{-5} & -4.3634\times10^{-4} & 1.6421\times10^{-4} & -1.9848\times10^{-4} \\ 6.8806\times10^{-5} & 3.7586\times10^{-5} & -1.3438\times10^{-4} & -5.9539\times10^{-5} & 8.9331\times10^{-4} & -7.3941\times10^{-5} & -1.7964\times10^{-4} & -5.0259\times10^{-4} & 4.6802\times10^{-4} \\ -4.0446\times10^{-5} & -9.4411\times10^{-6} & 7.3451\times10^{-5} & 3.5526\times10^{-5} & -7.3941\times10^{-5} & 9.7590\times10^{-4} & 0.0015 & -2.9611\times10^{-5} & -0.0010 \\ 0.0029 & 0.0031 & 0.0031 & -4.3634\times10^{-4} & -1.7964\times10^{-4} & 0.0015 & 0.0351 & 0.0064 & 0.0079 \\ 0.0038 & 0.0024 & 0.0033 & 1.6421\times10^{-4} & -5.0259\times10^{-4} & -2.9611\times10^{-5} & 0.0064 & 0.0383 & 0.0032 \\ 0.0046 & 0.0036 & 0.0016 & -1.9848\times10^{-4} & 4.6802\times10^{-4} & -0.0010 & 0.0079 & 0.0032 & 0.0365 \end{bmatrix} \tag{27}$$

$$P_2 = \begin{bmatrix} 0.0096 & 3.7995\times10^{-4} & 5.4754\times10^{-4} & 1.5132\times10^{-4} & 2.3001\times10^{-6} & 4.2492\times10^{-5} & 0.0032 & 0.0042 & 0.0045 \\ 3.7995\times10^{-4} & 0.0095 & 9.6141\times10^{-4} & -1.2578\times10^{-4} & 1.1375\times10^{-4} & -7.6911\times10^{-5} & 0.0047 & 0.0037 & 0.0058 \\ 5.4754\times10^{-4} & 9.6141\times10^{-4} & 0.0089 & 3.2388\times10^{-5} & -1.7169\times10^{-4} & 4.1692\times10^{-5} & 0.0046 & 0.0042 & 0.0023 \\ 1.5132\times10^{-4} & -1.2578\times10^{-4} & 3.2388\times10^{-5} & 6.3074\times10^{-4} & 1.5749\times10^{-4} & -1.0167\times10^{-4} & -5.6301\times10^{-5} & 4.1265\times10^{-4} & 1.5879\times10^{-4} \\ 2.3001\times10^{-6} & 1.1375\times10^{-4} & -1.7169\times10^{-4} & 1.5749\times10^{-4} & 0.0010 & -1.1159\times10^{-4} & 3.5998\times10^{-4} & -0.0012 & 2.8246\times10^{-4} \\ 4.2492\times10^{-5} & -7.6911\times10^{-5} & 4.1692\times10^{-5} & -1.0167\times10^{-4} & -1.1159\times10^{-4} & 0.0013 & 0.0019 & 1.4111\times10^{-4} & -0.0019 \\ 0.0032 & 0.0047 & 0.0046 & -5.6301\times10^{-5} & 3.5998\times10^{-4} & 0.0019 & 0.0500 & 0.0096 & 0.0035 \\ 0.0042 & 0.0037 & 0.0042 & 4.1265\times10^{-4} & -0.0012 & 1.4111\times10^{-4} & 0.0096 & 0.0439 & 0.0115 \\ 0.0045 & 0.0058 & 0.0023 & 1.5879\times10^{-4} & 2.8246\times10^{-4} & -0.0019 & 0.0035 & 0.0115 & 0.0479 \end{bmatrix} \tag{28}$$

$$P_3 = \begin{bmatrix} 0.0106 & -0.0011 & 9.1603\times10^{-4} & 8.8272\times10^{-6} & 2.6364\times10^{-4} & 6.1071\times10^{-5} & 0.0036 & 0.0030 & 0.0039 \\ -0.0011 & 0.0107 & 8.5566\times10^{-4} & 5.5040\times10^{-5} & 8.3071\times10^{-5} & -2.4789\times10^{-4} & 0.0030 & 0.0036 & 0.0044 \\ 9.1603\times10^{-4} & 8.5566\times10^{-4} & 0.0094 & -4.6809\times10^{-5} & -2.2394\times10^{-4} & 1.2699\times10^{-4} & 0.0063 & 0.0060 & 0.0037 \\ 8.8272\times10^{-6} & 5.5040\times10^{-5} & -4.6809\times10^{-5} & 0.0012 & -1.6796\times10^{-4} & -1.4031\times10^{-4} & -1.8414\times10^{-4} & 8.7477\times10^{-5} & 2.2478\times10^{-4} \\ 2.6364\times10^{-4} & 8.3071\times10^{-5} & -2.2394\times10^{-4} & -1.6796\times10^{-4} & 9.9333\times10^{-4} & 1.2144\times10^{-4} & 0.0011 & -0.0013 & 0.0011 \\ 6.1071\times10^{-5} & -2.4789\times10^{-4} & 1.2699\times10^{-4} & -1.4031\times10^{-4} & 1.2144\times10^{-4} & 0.0013 & 0.0021 & -9.8096\times10^{-4} & -0.0019 \\ 0.0036 & 0.0030 & 0.0063 & -1.8414\times10^{-4} & 0.0011 & 0.0021 & 0.0650 & -0.0132 & 0.0115 \\ 0.0030 & 0.0036 & 0.0060 & 8.7477\times10^{-5} & -0.0013 & -9.8096\times10^{-4} & -0.0132 & 0.0658 & 0.0101 \\ 0.0039 & 0.0044 & 0.0037 & 2.2478\times10^{-4} & 0.0011 & -0.0019 & 0.0115 & 0.0101 & 0.0452 \end{bmatrix} \tag{29}$$

REFERENCES

[1] R. H. Lasseter, "MicroGrids," in *Proc. IEEE Power Eng. Soc. Winter Meeting. Conf. Proc.* vol. 1, 2002, pp. 305–308.

[2] H. Kakigano, Y. Miura, and T. Ise, "Low-voltage bipolar-type DC microgrid for super high quality distribution," *IEEE Trans. Power Electron.*, vol. 25, no. 12, pp. 3066–3075, Dec. 2010.

[3] T. Dragičević, X. Lu, J. C. Vasquez, and J. M. Guerrero, "DC microgrids—Part II: A review of power architectures, applications, and standardization issues," *IEEE Trans. Power Electron.*, vol. 31, no. 5, pp. 3528–3549, May. 2016.

[4] D. Boroyevich, I. Cvetkovic, R. Burgos, and D. Dong, "Intergrid: A future electronic energy network?," *IEEE J. Emerg. Sel. Topics Power Electron.*, vol. 1, no. 3, pp. 127–138, Sep. 2013.

[5] Z. Li, M. Shahidehpour, F. Aminifar, A. Alabdulwahab, and Y. Al-Turki, "Networked microgrids for enhancing the power system resilience," *Proc. IEEE*, vol. 105, no. 7, pp. 1289–1310, Jul. 2017.

[6] X. Li *et al.*., "Flexible interlinking and coordinated power control of multiple DC microgrids clusters," *IEEE Trans. Sustain. Energy*, vol. 9, no. 2, pp. 904–915, Apr. 2018.

[7] L. Meng *et al.*., "Review on control of DC microgrids and multiple microgrid clusters," *IEEE J. Emerg. Sel. Topics Power Electron.*, vol. 5, no. 3, pp. 928–948, Sep. 2017.

[8] M. Nasir, Z. Jin, H. A. Khan, N. A. Zaffar, J. C. Vasquez, and J. M. Guerrero, "A decentralized control architecture applied to DC nanogrid clusters for rural electrification in developing regions," *IEEE Trans. Power Electron.*, vol. 34, no. 2, pp. 1773–1785, Feb. 2019.

[9] F. Chang, X. Cui, M. Wang, W. Su, and A. Q. Huang, "Large-signal stability criteria in DC power grids with distributed-controlled converters and constant power loads," *IEEE Trans. Smart Grid*, vol. 11, no. 6, pp. 5273–5287, Nov. 2020.

[10] W. Xie, M. Han, W. Cao, J. M. Guerrero, and J. C. Vasquez, "System-level large-signal stability analysis of droop-controlled DC microgrids," *IEEE Trans. Power Electron.*, vol. 36, no. 4, pp. 4224–4236, Apr. 2021.

[11] S. Liu, J. Zheng, R. Li, X. Li, W. Fang, and X. Liu, "Multiple Lyapunov function-based large signal stability analysis of DC microgrid with coordinated control," in *Proc. 22nd Int. Conf. Elect. Machines Syst. (ICEMS)*, 2019, pp. 1–6.

[12] R. Han, M. Tucci, A. Martinelli, J. M. Guerrero, and G. Ferrari-Trecate, "Stability analysis of primary plug-and-play and secondary leader-based controllers for DC microgrid clusters," *IEEE Trans. Power Syst.*, vol. 34, no. 3, pp. 1780–1800, May. 2019.

[13] Q. Shafiee, T. Dragicevic, J. C. Vasquez, and J. M. Guerrero, "Modeling, stability analysis and active stabilization of multiple DC-microgrid clusters," in *Proc. IEEE Int. Energy Conf. (ENERGYCON)*, 2014, pp. 1284–1290.

[14] J. He, X. Wu, X. Wu, Y. Xu, and J. M. Guerrero, "Small-signal stability analysis and optimal parameters design of microgrid clusters," *IEEE Access*, vol. 7, pp. 36896–36909, 2019.

[15] M. Belkhayat, R. Cooley, and A. Witulski, "Large signal stability criteria for distributed systems with constant power loads," in *Proc. PESC '95—Power Electron. Specialist Conf.*, vol. 2, 1995, pp. 1333–1338.

[16] D. Marx, P. Magne, B. Nahid-Mobarakeh, S. Pierfederici, and B. Davat, "Large signal stability analysis tools in DC power systems with constant power loads and variable power Loads—A review," *IEEE Trans. Power Electron.*, vol. 27, no. 4, pp. 1773–1787, Apr. 2012.

[17] J. Jiang *et al.*., "A conservatism-free large signal stability analysis method for DC microgrid based on mixed potential theory," *IEEE Trans. Power Electron.*, vol. 34, no. 11, pp. 11342–11351, Nov. 2019.

[18] M. Su, Z. Liu, Y. Sun, H. Han, and X. Hou, "Stability analysis and stabilization methods of DC microgrid with multiple parallel-connected DC–DC converters loaded by CPLs," *IEEE Trans. Smart Grid*, vol. 9, no. 1, pp. 132–142, Jan. 2018.

[19] Z. Li, W. Pei, H. Ye, and L. Kong, "Large signal stability analysis for DC microgrid under droop control based on mixed potential theory," *J. Eng.*, vol. 2019, no. 16, pp. 1189–1193, 2019.

[20] S. Sanchez and M. Molinas, "Large signal stability analysis at the common coupling point of a DC microgrid: A grid impedance estimation approach based on a recursive method," *IEEE Trans. Energy Convers.*, vol. 30, no. 1, pp. 122–131, Mar. 2015.

[21] A. P. N. Tahim, D. J. Pagano, E. Lenz, and V. Stramosk, "Modeling and stability analysis of islanded DC microgrids under droop control," *IEEE Trans. Power Electron.*, vol. 30, no. 8, pp. 4597–4607, Aug. 2015.

[22] J. Liu, W. Zhang, and G. Rizzoni, "Robust stability analysis of DC microgrids with constant power loads," *IEEE Trans. Power Syst.*, vol. 33, no. 1, pp. 851–860, Jan. 2018.

[23] D. Marx, S. Pierfederici, B. Nahid-Mobarakeh, and B. Davat, "Contribution to determination of domain of attraction in power systems: Application to drives with input filter," in *Proc. IEEE Ind. Appl. Soc. Annu. Meeting*, 2009, pp. 1–8.

[24] P. Karlsson and J. Svensson, "DC bus voltage control for a distributed power system," *IEEE Trans. Power Electron.*, vol. 18, no. 6, pp. 1405–1412, Nov. 2003.

[25] A. Emadi, A. Khaligh, C. H. Rivetta, and G. A. Williamson, "Constant power loads and negative impedance instability in automotive systems: Definition, modeling, stability, and control of power electronic converters and motor drives," *IEEE Trans. Veh. Technol.*, vol. 55, no. 4, pp. 1112–1125, Jul. 2006.

[26] A. M. Rahimi and A. Emadi, "Active damping in DC/DC power electronic converters: A novel method to overcome the problems of constant power loads," *IEEE Trans. Ind. Electron.*, vol. 56, no. 5, pp. 1428–1439, May. 2009.

[27] Q. Shafiee, T. Dragičević, J. C. Vasquez, and J. M. Guerrero, "Hierarchical control for multiple DC-Microgrids clusters," *IEEE Trans. Energy Convers.*, vol. 29, no. 4, pp. 922–933, Dec. 2014.

[28] X. Liu and Y. Bian, "Large signal stability analysis of the DC microgrid with the storage system," in *Proc. 20th Int. Conf. Elect. Machines Syst. (ICEMS),* 2017, pp. 1–5.

[29] T. Takagi and M. Sugeno, "Fuzzy identification of systems and its applications to modeling and control," *IEEE Trans. Syst., Man, Cybern.*, vol. SMC-15, no. 1, pp. 116–132, Jan./Feb. 1985.

[30] K. Tanaka and M. Sugeno, "Stability analysis and design of fuzzy control systems," *Fuzzy Sets Syst.*, vol. 45, no. 2, pp. 135–156, 1992.

[31] H. O. Wang, K. Tanaka, and M. F. Griffin, "An approach to fuzzy control of nonlinear systems: Stability and design issues," *IEEE Trans. Fuzzy Syst.*, vol. 4, no. 1, pp. 14–23, Feb. 1996.

[32] Y. Blanco, W. Perruquetti, and P. Borne, "Stability and stabilization of nonlinear systems and Takagi-Sugeno's fuzzy models," *Math. Problems Eng.*, vol. 7, pp. 221–240, 2001.

[33] H. Kim, S. Kang, G. Seo, P. Jang, and B. Cho, "Large-signal stability analysis of DC power system with shunt active damper," *IEEE Trans. Ind. Electron.*, vol. 63, no. 10, pp. 6270–6280, Oct. 2016.

Sucheng Liu (Member, IEEE) received the Ph.D. degree in electrical engineering from Chongqing University, Chongqing, China, in 2013.

He was a Lecturer with the Department of Electrical Engineering, Anhui University of Technology, Ma'anshan, China, from 2013 to 2016, and has been an Associate Professor, since 2016. He was a Visiting Research Associate with Queen's University, Kingston, ON, Canada, where he conducted two research projects sponsored by GE and NSERC, from 2015 to 2016. His research interests include modeling and control of dc microgrids and clusters, and design of switching power converters. He has authored or coauthored more than 40 refereed journal and conference papers and holds seven patents and has eight patents pending.

Dr. Liu is a member of the IEEE Power Electronics Society. He has also been an Active Reviewer for a dozen of international journals and conferences, such as IEEE TRANSACTIONS ON POWER ELECTRONICS, IEEE JOURNAL OF EMERGING AND SELECTED TOPICS IN POWER ELECTRONICS, IEEE OPEN JOURNAL OF POWER ELECTRONICS, IEEE TRANSACTIONS ON INDUSTRIAL ELECTRONICS, IET Power Electronics, *International Journal of Electrical Power and Energy Systems, Electric Power Components and Systems, International Journal of Electronics*, APEC, ECCE, ECCE Asia, etc. He was a TPC Member of IEEE IPEC-Niigata 2018, and a Session Chair for IEEE WiPDA-Asia, CPSSC, and SPEED. He was the recipient of Best Paper Awards at the IEEE International Conference on DC Microgrids (ICDCM), Matsue, Japan, in 2019, and The China Power Supply Society Conference (CPSSC), Shanghai, China, in 2017.

Xiang Li (Student Member, IEEE) was born in Anhui, China, in 1996. He received the B.S. degree in electrical engineering and automation in 2019 from Anhui University of Technology, Ma'anshan, China, where he is currently working toward the M.S. degree in electrical engineering.

His research interests include stability analysis and control of dc microgrids systems. He has authored or coauthored three refereed conference papers and holds one patent and has three patents pending.

Mengyu Xia (Student Member, IEEE) was born in Anhui, China, in 1998. He received the B.S. degree in electrical engineering and automation in 2019 from Anhui University of Technology, Ma'anshan, China, where he is currently working toward the M.S. degree in electrical engineering.

His research interests include communications and cyber security of dc microgrids systems. He has authored or coauthored two refereed conference papers and has one patent pending.

Qiangdong Qin (Student Member, IEEE) was born in Shanxi, China, in 1996. He received the B.S. degree in electrical engineering and automation in 2019 from Anhui University of Technology, Ma'anshan, China, where he is currently working toward the M.S. degree in electrical engineering.

His research interests include predictive control of dc microgrids systems. He has authored or coauthored one refereed conference paper and has three patents pending.

Xiaodong Liu was born in Jilin, China, in 1971. He received the Ph.D. degree in electric machines and electric apparatus from Zhejiang University, Hangzhou, China, in 1999.

Since 2003, he has been with the School of Electrical and Information Engineering, Anhui University of Technology, Ma'anshan, China, where he is currently a Full Professor. He was a Visiting Scholar with Queen's University, Kinston, ON, Canada, from July to October 2007. His research interests include the dc-dc switching converter, power factor correction techniques, and motor design and driving control.